

# Higher fully-charmed tetraquarks: Radial excitations and P-wave states

Guang-Juan Wang,<sup>1</sup> Lu Meng,<sup>2,\*</sup> Makoto Oka,<sup>1,3,†</sup> and Shi-Lin Zhu<sup>4,‡</sup>

<sup>1</sup>*Advanced Science Research Center, Japan Atomic Energy Agency, Tokai, Ibaraki, 319-1195, Japan*

<sup>2</sup>*Institut für Theoretische Physik II, Ruhr-Universität Bochum, D-44780 Bochum, Germany*

<sup>3</sup>*Nishina Center for Accelerator-Based Science, RIKEN, Wako 351-0198, Japan*

<sup>4</sup>*School of Physics and Center of High Energy Physics, Peking University, Beijing 100871, China*

We systematically calculate the mass spectrum of the higher excited fully-charmed tetraquark  $cc\bar{c}\bar{c}$  states including the S-wave radial excitations and the P-wave states with a nonrelativistic quark model. The quark model is composed of a vector one-gluon-exchange (OGE) and a scalar linear confinement interaction with the parameters determined by the charmonium spectrum. In the calculation, we consider both the  $3_c - \bar{3}_c$  and the  $6_c - \bar{6}_c$  color representations. For the  $cc\bar{c}\bar{c}$  state, the  $6_c - \bar{6}_c$  component is located lower than the  $\bar{3}_c - 3_c$  one because of the stronger attractive interactions between the diquark and antidiquark. We focus on two excited modes and their properties for the P-wave tetraquarks. The mass splitting for the  $\rho$ -mode excitations with different color configurations is large. The low-lying  $6_c - \bar{6}_c$   $\rho$ -mode component helps to explain the small mass gap between the ground S-wave and the P-wave tetraquark states. The recently observed  $X(6900)$  state may be the candidate of the first radially excited tetraquarks with  $J^{PC} = 0^{++}$  or  $2^{++}$ , or the  $1^{+-}$  or  $2^{-+}$  P-wave states based on the mass spectrum. Moreover, the lowest  $T_c$  states with the exotic  $J^{PC}$  quantum numbers  $0^{--}$  and  $1^{--}$  may decay into the P-wave  $\eta_c J/\psi$  and di- $J/\psi$  modes, respectively. The future experimental search of these  $T_c$  states will enrich the hadronic spectrum.

## I. INTRODUCTION

Since 2003, dozens of the exotic states named as XYZ states were discovered in the mass range of the heavy quarkonium in experiments. Amounts of them cannot be categorized as the conventional  $Q\bar{Q}$  ( $Q = b, c$ ) mesons, and are candidates of the multi-quark states  $QQq\bar{q}$  based on their quantum numbers (for example, charge and  $J^{PC}$ ) and decay channels. Various interpretations have been proposed for their nature, including the hadronic molecule, the compact tetraquark, the hadro-charmonium, and so on (for recent reviews, see Refs. [1–8]). However, none of the exotic states have been firmly established so far.

The light quark degrees of freedom in the XYZ state make the investigation of their nature very complicated. Two heavy hadrons can form the loosely bound molecules by exchanging light mesons such as the deuteron ( $P_c$  states are also the good candidates of molecules [9, 10]). Alternatively, the four quarks form a compact tetraquark state through the colored force. Moreover, the  $QQq\bar{q}$  states might strongly couple to the  $Q\bar{Q}$  core when their masses approach each other [11].

In contrast, the fully heavy tetraquark does not contain any light quarks. The light-meson-exchange interaction between two charmonia is suppressed, while the heavy quarks could be bound through the short-range colored forces arising from the gluon-exchange interaction in QCD. Thus, they are more likely to be candidates of the compact tetraquark states instead of the molecules. Moreover, the fully heavy tetraquark states

lie very far away from the conventional heavy quarkonium states, which suppresses the coupled-channel effect between the tetraquark components and the  $Q\bar{Q}$  core. Thus, the fully heavy tetraquark state becomes a golden platform for the study of the multi-quark states.

Before the experimental observation, there exist lots of theoretical studies about the fully-heavy tetraquark states in literature [12–17]. Recently, the CMS [18, 19] and the LHCb [20] searched the fully-bottom state  $X_{bb\bar{b}\bar{b}}$  in the  $\Upsilon(1S)\mu^+\mu^-$  channel. An analysis using CMS data reported an excess in this channel [19]. The experimental processes inspired the intensive discussions [21–37]. These theoretical works focus on the existence of the stable bound state below the lowest di-heavy-quarkonium threshold. Some theoretical works support the existence of the bound tetraquark [21–29], while others do not favor it [14, 30–34]. Very recently, the LHCb collaboration searched the di- $J/\psi$  channel and reported a broad structure in the mass region (6.2, 6.8) GeV and a narrow  $X(6900)$  state with the signal significance more than  $5\sigma$  [38]. The experimental results inspired numerous theoretical discussions [39–86]. The most popular interpretations are the compact tetraquark states [39–50]. Other rare interpretations, such as coupled-channel effects of double-charmonium channels [51, 52],  $c\bar{c}$  hybrid [53], a Higgs-like boson [54] and so on, are also proposed. The interpretations of their nature are still in debate. Other properties, for instance, the production mechanisms [55–61] and the decay patterns [42, 62, 63] have also been discussed.

In our previous work before the observation of  $X(6900)$  [37], we calculated the fully heavy tetraquark states. We found that the ground S-wave  $cc\bar{c}\bar{c}$  (noted as  $T_c$  here and after) states are located around (6.3, 6.5) GeV. Meanwhile, we also predicted several radially excited states around 6.9 GeV, which are consistent with

\* lu.meng@rub.de

† oka@post.j-parc.jp

‡ zhushl@pku.edu.cn

the  $X(6900)$  observed in LHCb. In Refs. [35, 40], the P-wave  $T_c$  states were also predicted about 6.9 GeV. For the P-wave excited compact tetraquarks, one should include the spin-orbital and tensor potentials in the quark model. Moreover, the P-wave excitation may appear within the diquark/anti-diquark clusters or between two clusters. Both the potentials and the possible excitation modes make the P-wave state much more complicated than the S-wave ones. In this work, we will refine and extend our investigation on the fully-charmed  $cc\bar{c}\bar{c}$  states in the compact tetraquark model. We will perform a dynamical calculation for the mass spectrum of the higher tetraquark states, including the S-wave radial excitations and the P-wave states with two excitation modes.

To study the mass spectrum of the  $T_c$  states, we adopt the nonrelativistic quark model with the minimal heavy quark interaction which could describe charmonium spectrum. The potential contains the one-gluon-exchange (OGE) Coulomb-like, the linear confinement, and the hyperfine interactions. The short-range spin-orbital and tensor potentials arising from the OGE force and a long-range spin-orbital interaction arising from the linear confinement term are treated perturbatively. The color wave functions of the conventional mesons and baryons are uniquely determined. However, there are two possible color configurations for the  $T_c$  state, the  $\bar{3}_c - 3_c$  and  $6_c - \bar{6}_c$ . In this work, we include both of the two color configurations. With the careful treatment of the mixing effects, we systematically calculate the  $T_c$  mass spectra and investigate their inner structures.

The paper is organized as follows. In Sec. II, we introduce the Hamiltonian and construct the wave functions of the tetraquark states. In Sec. III and Sec. IV, we present the mass spectra and details for S-wave and P-wave tetraquark states in order. We provide the lower lying decay channels to search them in Sec. V. In Sec. VI, we adopt the harmonic oscillator potential to qualitatively explain the small mass splitting between the S-wave and P-wave  $T_c$  states. Finally, we give a brief summary in Sec. VII. In Appendix, we give the spin, spin-orbital and tensor factors used in the calculation.

## II. HAMILTONIAN AND WAVE FUNCTION

For the fully heavy tetraquark state, we employ the non-relativistic quark model proposed in Ref. [87]. The potentials are composed of the one-gluon-exchange potential  $[G(q^2)(\gamma_\mu)_q \otimes (\gamma^\mu)_{\bar{q}}]$  and a phenomenological linear confinement potential  $[S(Q^2)(1)_q(1)_{\bar{q}}]$  (where  $G(Q^2)$  and  $S(Q^2)$  are given in Ref. [88]). The Hamiltonian reads

$$\begin{aligned} H &= H_0 + V^{(0)} + V^{(1)}, \\ H_0 &= \sum_{i=1}^4 \frac{\mathbf{p}_i^2}{2m_i} + \sum_i m_i - T_G, \\ V^{(0)} &= \frac{\lambda_i}{2} \cdot \frac{\lambda_j}{2} V_{\text{cen}}(r_{ij}), \end{aligned}$$

$$V^{(1)} = \frac{\lambda_i}{2} \cdot \frac{\lambda_j}{2} [V_{\text{so}}(r_{ij}) + V_{\text{tens}}(r_{ij})], \quad (1)$$

where  $\mathbf{p}_i$  and  $m_i$  denote the momentum and mass of the  $i$ th (anti)quark. The kinematic energy of the system  $T_G$  vanishes in the center mass system of the  $T_c$  state.  $\lambda_i$  is the color matrix. We divide the interaction into the leading interaction  $V^{(0)}$  and the perturbation  $V^{(1)}$ . The leading central potential  $V_{\text{cen}}(r_{ij})$  is composed of the OGE Coulomb-like  $V_{\text{Coul}}$ , linear confinement  $V_{\text{lin}}$  and screened hyperfine interactions  $V_{\text{hyp}}$ ,

$$\begin{aligned} V_{\text{cen}}(r_{ij}) &= V_{\text{Coul}} + V_{\text{lin}} + V_{\text{hyp}} \\ &= \frac{\alpha_s}{r_{ij}} - \frac{3}{4}br_{ij} - \frac{8\pi\alpha_s}{3m_im_j} \left( \frac{\sigma}{\sqrt{\pi}} \right)^3 e^{-\sigma^2 r_{ij}^2} \mathbf{s}_i \cdot \mathbf{s}_j. \end{aligned} \quad (2)$$

For the orbitally excited states, the remaining perturbation, spin-orbital potential  $V_{\text{so}}$  and tensor potential  $V_{\text{tens}}$  may shift the mass spectrum obtained with the leading interaction  $V^{(0)}$ . Their explicit forms are

$$\begin{aligned} V_{\text{so}}(r_{ij}) &= V_{\text{so}}^v(r_{ij}) + V_{\text{so}}^s(r_{ij}), \\ V_{\text{so}}^v(r_{ij}) &= \frac{1}{r_{ij}} \frac{dV_{\text{Coul}}}{dr_{ij}} \frac{1}{4} \left[ \left( \frac{1}{m_i^2} + \frac{1}{m_j^2} + \frac{4}{m_im_j} \right) \mathbf{L}_{ij} \cdot \mathbf{S}_{ij} \right. \\ &\quad \left. + \left( \frac{1}{m_i^2} - \frac{1}{m_j^2} \right) \mathbf{L}_{ij} \cdot (\mathbf{s}_i - \mathbf{s}_j) \right], \\ V_{\text{so}}^s(r_{ij}) &= -\frac{1}{r_{ij}} \frac{dV_{\text{lin}}}{dr_{ij}} \left( \frac{\mathbf{L}_{ij} \cdot \mathbf{s}_i}{2m_i^2} + \frac{\mathbf{L}_{ij} \cdot \mathbf{s}_j}{2m_j^2} \right), \\ V_{\text{tens}}(r_{ij}) &= -\left( \frac{\partial^2}{\partial r_{ij}^2} - \frac{1}{r_{ij}} \frac{\partial}{\partial r_{ij}} \right) \frac{V_{\text{Coul}}}{3m_im_j} \mathcal{S}_{ij}, \end{aligned} \quad (3)$$

where  $\mathbf{s}_i$  is the spin operator for the  $i$ th (anti)quark.  $\mathbf{S}_{ij} = \mathbf{s}_i + \mathbf{s}_j$  is the spin operator for the  $(ij)$ th (anti)quark pair. The relative orbital operators  $\mathbf{L}_{ij}$  is defined as

$$\mathbf{L}_{ij} = \mathbf{r}_{ij} \times \mathbf{p}_{ij} = \mathbf{r}_{ij} \times \frac{m_i \mathbf{p}_i - m_j \mathbf{p}_j}{m_i + m_j}. \quad (4)$$

The tensor operator  $\mathcal{S}_{ij}$  reads

$$\mathcal{S}_{ij} = \frac{3(\mathbf{s}_i \cdot \mathbf{r}_{ij})(\mathbf{s}_j \cdot \mathbf{r}_{ij})}{r_{ij}^2} - \mathbf{s}_i \cdot \mathbf{s}_j. \quad (5)$$

The  $V_{\text{so}}^v(r_{ij})$  and  $V_{\text{tens}}(r_{ij})$  are given as relativistic corrections from the one-gluon-exchange potential as illustrated in Appendix A of Ref. [88] and thus related to the OGE Coulomb-like potential  $V_{\text{Coul}}$ . The  $V_{\text{so}}^s(r_{ij})$  arises from the linear confinement potential  $V_{\text{lin}}$ . In the calculation, we treat the potential  $V_{\text{cen}}(r_{ij})$  as the leading effects and consider the remaining spin-orbital and tensor effects as the perturbation to shift the mass spectrum. We solve the Schrödinger equation for the mesons and tetraquarks in two stages. In the first stage, we include the potential  $V^{(0)}$  in the Hamiltonian and solve the Schrödinger equation with the variational method to

TABLE I. The parameters of the quark model and the corresponding mass spectrum (THE) of the charmonia  $c\bar{c}$  compared with their experimental values (EXP) [89].

parameter		Mass spectrum (MeV)			
		$^{2S+1}L_J$	Meson	EXP	THE
$\alpha_s$	0.5461	$^1S_0$	$\eta_c$	2983.9	2984
$b$ [GeV <sup>2</sup> ]	0.1452	$^3S_1$	$J/\psi$	3096.9	3092
$m_c$ [GeV]	1.4794	$^3P_0$	$\chi_{c0}$	3414.7	3426
$\sigma$ [GeV]	1.0946	$^3P_1$	$\chi_{c1}$	3510.7	3506
		$^1P_1$	$h_c(1P)$	3525.4	3516
		$^3P_2$	$\chi_{c2}$	3556.2	3556
		$^1S_0$	$\eta_c(2S)$	3637.5	3634
		$^3S_1$	$\psi(2S)$	3686.1	3675
		$^3S_1$	$\psi(3S)$	4039.0	4076
		$^3S_1$	$\psi(4S)$	4421.0	4412

obtain the eigenstates. In the second stage, we consider the potential  $V^{(0)} + V^{(1)}$  in the Hamiltonian and calculate the mass spectrum by diagonalizing the Hamiltonian matrix in the basis of eigenstates obtained in the first stage, where only the  $V^{(0)}$  is considered. As a benchmark, we calculate the mass spectrum of the low-lying S-wave and P-wave charmonium with the parameters in Ref. [87]. The results are summarized in Table I. The quark model reproduces the experimental values successfully. The deviations from the experimental data are about 10 MeV or even smaller, except that for the third radially excited state  $\psi(3S)$ , which is 37 MeV.

The four-quark system  $T_c$  can be described by three independent coordinates shown in Fig. 1. Corresponding to the two sets of Jacobi coordinates, one has two methods to neutralize the state in the color space,  $|(Q_1 Q_2)_{\bar{3}_c}(\bar{Q}_3 \bar{Q}_4)_{3_c}\rangle$  and  $|(Q_1 Q_2)_{6_c}(\bar{Q}_3 \bar{Q}_4)_{\bar{6}_c}\rangle$  for the left diagram, while  $|(Q_1 \bar{Q}_3)_{8_c}(Q_2 \bar{Q}_4)_{8_c}\rangle$  and  $|(Q_1 \bar{Q}_3)_{1_c}(Q_2 \bar{Q}_4)_{1_c}\rangle$  ( $Q_1 \leftrightarrow Q_2$  or  $Q_3 \leftrightarrow \bar{Q}_4$ ) for the right one. The two sets are equivalent to each other, which can be proved by the Fierz transformation if one considers the complete spatial expansion basis [37]. With the left set of Jacobi coordinates, we can directly include the Fermi statistic constraints on the quarks and antiquarks as listed in Table II, which simplifies the calculation. Thus, we expand the tetraquark state with the Gaussian wave functions in the basis of the left Jacobi coordinates [90, 91]. The wave functions of the  $T_c$  state with the angular momentum  $(J, J_z)$  read,

$$\Psi_{JJ_z} = \sum_{\alpha} A_{\alpha} \cdot \chi_c \phi_{n_a l_a}(r_{12}, \beta_a) \phi_{n_b l_b}(r_{34}, \beta_b) \phi_{n_{ab} l_{ab}}(r, \beta) \cdot \left[ [(Y_{l_a}(\hat{r}_{12}) \otimes \chi_{s_a})_{j_a} (Y_{l_b}(\hat{r}_{34}) \otimes \chi_{s_b})_{j_b}]_j \otimes Y_{l_{ab}}(\hat{r}) \right]_{JJ_z}, \quad (6)$$

where the spatial wave function reads

$$\phi_{n_a l_a}(r_{12}, \beta_a) = \left\{ \frac{2^{l_a+2} (2\nu_{n_a})^{l_a+3/2}}{\sqrt{\pi} (2l_a+1)!!} \right\}^{1/2} r_{12}^{l_a} e^{-\nu_{n_a} r_{12}^2},$$

with  $\nu_{n_a}$  being the oscillating parameter,

$$\nu_{n_a} = \frac{n_a \beta_a^2}{2}, \quad (n_a = 1, 2, \dots, n_a^{\max}), \quad (7)$$

The  $n_a/n_b/n_{ab}$  are related to the radial excitations along the three relative coordinates.  $l_a/l_b/l_{ab}$  are the orbital angular momenta inside the diquark/antidiquarks, and that between the two clusters, respectively. The spin of the diquark (antidiquarks)  $s_a$  ( $s_b$ ) couples with  $l_a$  ( $l_b$ ) into the  $j_a$  ( $j_b$ ).  $j_a$  and  $j_b$  couple into  $j$  and then combine with  $l_{ab}$  to form the total angular momentum  $J$ . The  $\alpha$  represents the basis with the quantum number  $\{n_a, l_a, s_a, j_a, n_b, l_b, s_b, j_b, n_{ab}, l_{ab}, j\}$  which can form the angular momentum  $J$ . The expanding parameter  $A_{\alpha}$  and the oscillating parameters  $\beta_{a/b/ab}$  are determined by solving the Schrödinger equation with the variational method.

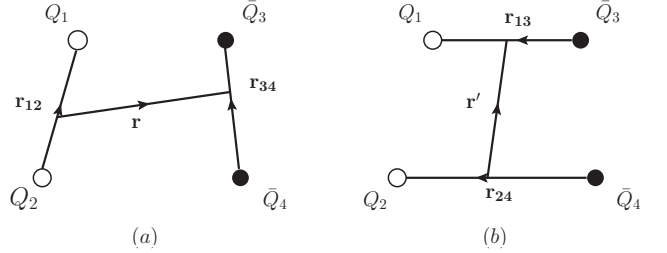


FIG. 1. Two sets of Jacobi coordinates in the four-quark system. The  $Q_1/Q_2$  and  $\bar{Q}_3/\bar{Q}_4$  are the quarks and antiquarks, respectively. An equivalent Jacobi coordinate to the right one is the one under the permutation of  $Q_1 \leftrightarrow Q_2$  or  $Q_3 \leftrightarrow \bar{Q}_4$ .

The  $\chi_s$  and  $\chi_c$  stand for the spin and color wave functions, respectively. We present the possible color-flavor-spin configurations of the  $T_c$  state in Table III. For the P-wave state, there are two orbital excitation modes, the  $\rho$ -mode state with the orbital excitation in the diquark or antidiquark, i.e.,  $|l_a = 1, l_b = l_{ab} = 0\rangle$  or  $|l_a = 0, l_b = 1, l_{ab} = 0\rangle$ , and the  $\lambda$ -mode one with the orbital excitation between the two clusters, i.e.,  $|l_a = l_b = 0, l_{ab} = 1\rangle$ . In general, the state should be a superposition of the two modes.

### III. SPECTRUM OF S-WAVE TETRAQUARKS AND THEIR RADIAL EXCITATIONS

The possible spin and parity quantum numbers of the S-wave  $T_c$  states are  $J^{PC} = 0^{++}, 1^{+-},$  and  $2^{++}$ . An S-wave tetraquark state may couple with the orbitally excited tetraquarks with at least two orbital angular momentum, i.e.,  $(l_a, l_b, l_{ab}) = (1, 1, 0), (0, 1, 1), (1, 1, 2),$  etc. For the  $T_c$  state, such orbital excited states will couple

TABLE II. The color-flavor-spin configurations of the  $QQ$  ( $\bar{Q}\bar{Q}$ ) diquark (antidiquark). The scripts “S” and “A” represent the exchange symmetry and antisymmetry for the identical particles, respectively.

Flavor	S-wave( $L = 0$ )	Spin	Color	$J^P$
S	S	$S(S_{QQ} = 1)$	$\bar{3}_c(\text{A})$	$[QQ]_{\bar{3}_c}^1 1^+$
S	S	$A(S_{QQ} = 0)$	$6_c(\text{S})$	$[QQ]_{6_c}^0 0^+$
Flavor	P-wave ( $L = 1$ )	Spin	Color	
S	A	$S(S_{QQ} = 1)$	$6_c(\text{S})$	$[[QQ]_{6_c}^1, \rho]_{6_c}^0 0^-$
				$[[QQ]_{6_c}^1, \rho]_{6_c}^1 1^-$
				$[[QQ]_{6_c}^1, \rho]_{6_c}^2 2^-$
S	A	$A(S_{QQ} = 0)$	$\bar{3}_c(\text{A})$	$[[QQ]_{\bar{3}_c}^0, \rho]_{\bar{3}_c}^1 1^-$

TABLE III. The color-flavor-spin wave functions of the S-wave and P-wave tetraquark states with different  $J^{PC}$ . The superscripts and subscripts in the wave functions represent the spin and the color representations, respectively. We use  $|c_{\rho/\lambda}^C; {}^{2S+1}P_J\rangle$  to label P-wave states, where  $c = 3$  or  $6$  stand for the color representation and  $C$  is the C-parity of the system.

S-wave	$0^{++}$	$[[QQ]_{\bar{3}_c}^1 [\bar{Q}\bar{Q}]_{\bar{3}_c}^1]_{1_c}^0$	$1^{+-}$	$[[QQ]_{\bar{3}_c}^1 [\bar{Q}\bar{Q}]_{\bar{3}_c}^1]_{1_c}^1$
		$[[QQ]_{6_c}^0 [\bar{Q}\bar{Q}]_{6_c}^0]_{1_c}^0$	$2^{++}$	$[[QQ]_{\bar{3}_c}^1 [\bar{Q}\bar{Q}]_{\bar{3}_c}^1]_{1_c}^2$
P-wave	$\lambda$ -mode		$\rho$ -mode	
	$0^{-+}$	$ 3_{\lambda}^{+,3} P_0\rangle = [[[[QQ]_{\bar{3}_c}^1 [\bar{Q}\bar{Q}]_{\bar{3}_c}^1]_{1_c}, \lambda]_{1_c}^0]$	$ 3_{\rho}^{+,3} P_0\rangle = \frac{1}{\sqrt{2}} \left( [[[[QQ]_{\bar{3}_c}^0, \rho]_{\bar{3}_c}^1 [\bar{Q}\bar{Q}]_{\bar{3}_c}^1]_{1_c}^0] + c.c. \right)$	
			$ 6_{\rho}^{+,3} P_0\rangle = \frac{1}{\sqrt{2}} \left( [[[[QQ]_{6_c}^1, \rho]_{6_c}^0 [\bar{Q}\bar{Q}]_{6_c}^0]_{1_c}^0] + c.c. \right)$	
	$1^{-+}$	$ 3_{\lambda}^{+,3} P_1\rangle = [[[[QQ]_{\bar{3}_c}^1 [\bar{Q}\bar{Q}]_{\bar{3}_c}^1]_{1_c}, \lambda]_{1_c}^1]$	$ 3_{\rho}^{+,3} P_1\rangle = \frac{1}{\sqrt{2}} \left( [[[[QQ]_{\bar{3}_c}^0, \rho]_{\bar{3}_c}^1 [\bar{Q}\bar{Q}]_{\bar{3}_c}^1]_{1_c}^1] + c.c. \right)$	
			$ 6_{\rho}^{+,3} P_1\rangle = \frac{1}{\sqrt{2}} \left( [[[[QQ]_{6_c}^1, \rho]_{6_c}^1 [\bar{Q}\bar{Q}]_{6_c}^0]_{1_c}^1] + c.c. \right)$	
	$2^{-+}$	$ 3_{\lambda}^{+,3} P_2\rangle = [[[[QQ]_{\bar{3}_c}^1 [\bar{Q}\bar{Q}]_{\bar{3}_c}^1]_{1_c}, \lambda]_{1_c}^2]$	$ 3_{\rho}^{+,3} P_2\rangle = \frac{1}{\sqrt{2}} \left( [[[[QQ]_{\bar{3}_c}^0, \rho]_{\bar{3}_c}^1 [\bar{Q}\bar{Q}]_{\bar{3}_c}^1]_{1_c}^2] + c.c. \right)$	
			$ 6_{\rho}^{+,3} P_2\rangle = \frac{1}{\sqrt{2}} \left( [[[[QQ]_{6_c}^1, \rho]_{6_c}^2 [\bar{Q}\bar{Q}]_{6_c}^0]_{1_c}^2] + c.c. \right)$	
	$0^{--}$	—	$ 3_{\rho}^{-,3} P_0\rangle = \frac{1}{\sqrt{2}} \left( [[[[QQ]_{\bar{3}_c}^0, \rho]_{\bar{3}_c}^1 [\bar{Q}\bar{Q}]_{\bar{3}_c}^1]_{1_c}^0] - c.c. \right)$	
			$ 6_{\rho}^{-,3} P_0\rangle = \frac{1}{\sqrt{2}} \left( [[[[QQ]_{6_c}^1, \rho]_{6_c}^0 [\bar{Q}\bar{Q}]_{6_c}^0]_{1_c}^0] - c.c. \right)$	
			$ 3_{\lambda}^{-,1} P_1\rangle = [[[[QQ]_{\bar{3}_c}^1 [\bar{Q}\bar{Q}]_{\bar{3}_c}^1]_{1_c}, \lambda]_{1_c}^1]$	
			$ 3_{\rho}^{-,3} P_1\rangle = \frac{1}{\sqrt{2}} \left( [[[[QQ]_{\bar{3}_c}^0, \rho]_{\bar{3}_c}^1 [\bar{Q}\bar{Q}]_{\bar{3}_c}^1]_{1_c}^1] - c.c. \right)$	
			$ 6_{\lambda}^{-,1} P_1\rangle = [[[[QQ]_{6_c}^0 [\bar{Q}\bar{Q}]_{6_c}^0]_{1_c}, \lambda]_{1_c}^1]$	
			$ 6_{\rho}^{-,3} P_1\rangle = \frac{1}{\sqrt{2}} \left( [[[[QQ]_{6_c}^1, \rho]_{6_c}^1 [\bar{Q}\bar{Q}]_{6_c}^0]_{1_c}^1] - c.c. \right)$	
			$ 3_{\lambda}^{-,5} P_1\rangle = [[[[QQ]_{\bar{3}_c}^1 [\bar{Q}\bar{Q}]_{\bar{3}_c}^1]_{1_c}, \lambda]_{1_c}^1]$	
			$ 3_{\rho}^{-,3} P_2\rangle = \frac{1}{\sqrt{2}} \left( [[[[QQ]_{\bar{3}_c}^0, \rho]_{\bar{3}_c}^1 [\bar{Q}\bar{Q}]_{\bar{3}_c}^1]_{1_c}^2] - c.c. \right)$	
	$2^{--}$	$ 3_{\lambda}^{-,5} P_2\rangle = [[[[QQ]_{\bar{3}_c}^1 [\bar{Q}\bar{Q}]_{\bar{3}_c}^1]_{1_c}, \lambda]_{1_c}^2]$	$ 6_{\rho}^{-,3} P_2\rangle = \frac{1}{\sqrt{2}} \left( [[[[QQ]_{6_c}^1, \rho]_{6_c}^2 [\bar{Q}\bar{Q}]_{6_c}^0]_{1_c}^2] - c.c. \right)$	
			$ 3_{\lambda}^{-,5} P_3\rangle = [[[[QQ]_{\bar{3}_c}^1 [\bar{Q}\bar{Q}]_{\bar{3}_c}^1]_{1_c}, \lambda]_{1_c}^3]$	

with the S-wave ones through spin-orbital and tensor potentials in Eq. (3), which could raise or lower the orbital momentum. Such interactions contribute to the mass shifting slightly. Thus, we do not include such high orbital excitations for the S-wave tetraquarks and concentrate on the state without any orbital angular momentum.

We present the results in Fig. 2 with the blue bars. For comparison, we also draw the results with the dot-dashed red bars using another quark model proposed in Ref. [92], which has been employed in our previous work [37]. In Fig. 2, one finds that the two sets of numerical results are similar to each other within tens of MeV for the low-lying excited states. For the higher radially excited states, the differences will become larger. This arises from the unavoidable uncertainties of quark model in the sector. Furthermore, the higher S-wave radially excited states might be located very close to the non-S-wave excited states, such as  $(l_a, l_b, l_{ab}) = (1, 1, 2)$ . The spin-orbital and tensor potentials will lead to their mixing effects. If their mass difference is small, even small contributions from the spin-orbital and tensor potentials may lead to large mixing. This will influence both the mass spectrum and the decay patterns. The mixing effect therefore cannot be neglected. Our present calculations are still robust for the low-lying tetraquark states. Additionally, the lowest  $T_c$  states are located above the lowest two-charmonium channels. We therefore conclude that there is no bound state for the  $T_c$  states, which is consistent with our conclusions in the previous work [37]. We also display the details of the S-wave states in Table IV, including the radius and the components of different color configurations. According to the radius, the four (anti)-quarks are confined into a compact state.

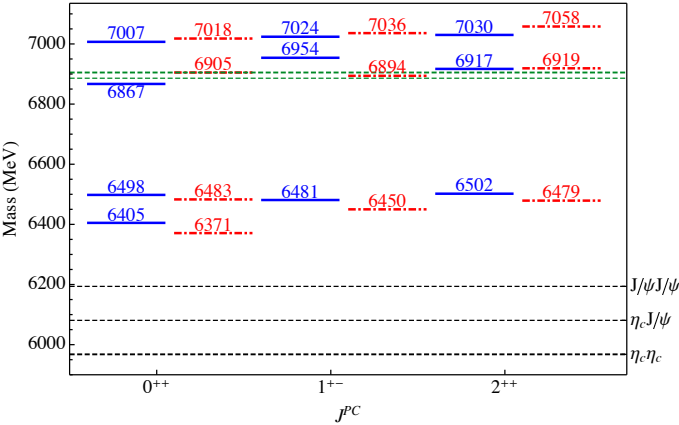


FIG. 2. The mass spectrum of the S-wave tetraquark states  $T_c$ . The dot-dashed red and the blue bars represent the mass spectra from the quark model in Ref. [92] and Ref. [87], respectively. The green dashed lines stand for 6886 MeV and 6905 MeV, which are the central values of the  $X(6900)$  mass in the two fits obtained by experiments [38].

#### IV. P-WAVE TETRAQUARK SPECTRUM

For the P-wave tetraquark, we consider the  $\rho$ -mode and the  $\lambda$ -mode tetraquarks with one orbital excitation. First, we calculate the eigenstates using the leading interactions, including the OGE Coulomb-like plus linear confinement, and the hyperfine potentials in Eq. (2).

As illustrated in Table III, the color-flavor-spin wave functions of the  $T_c$  states with  $J^{PC} = J^{-+}$  ( $J = 0, 1, 2$ ) are the same except for the total couplings of the spin and orbital angular momentum. With the leading Coulomb, confinement and hyperfine potentials, their mass spectrum are also the same. The mass difference comes from the perturbative spin-orbital or tensor potentials. This also applies to the  $T_c$ 's with the negative charge conjugate parity  $J^{--}$  ( $J = 1, 2, 3$ ) except for the  $1^{--}$  one, which has two extra  $\lambda$ -mode states. We list the eigenstates and corresponding percentages of different components under the leading potentials in Table V.

In the calculation, we find that the color electric interactions do not induce the mixing of the  $\lambda$ - and  $\rho$ -mode  $T_c$  excitations. From Table III, we can see that the spin wave functions are orthogonal for the  $\lambda$ - and  $\rho$ -mode constrained by the Fermi-Dirac statistics. Thus, the electric interactions do not mix the  $\lambda$ - and  $\rho$ -mode.

Next, we concentrate on the hyperfine interaction with the color magnetic operator. For the  $J^{PC} = 1^{--}$  and  $J^{PC} = 2^{--}$  tetraquarks, the total spin of the  $\lambda$ -mode states is 0 or 2 as shown in Table III, while that of the  $\rho$ -mode state is 1. The hyperfine potential cannot flip the total spin as

$$\langle [\chi_s^a \otimes \chi_s^b]^{S_\lambda=0/2} | \mathbf{s}_i \cdot \mathbf{s}_j | [\chi_s^a \otimes \chi_s^b]^{S_\rho=1} \rangle = 0, \quad (8)$$

where the subscripts  $a$  and  $b$  represent the diquark and antidiquark, respectively. For the  $J^{PC} = 0^{-+}, 1^{-+}, 2^{-+}$  tetraquarks, the hyperfine potentials will contribute to the mixing of the two P-wave excitation modes. The mixing is quite small and the eigenstates are nearly total  $\lambda$  or  $\rho$ -mode excitations. We denote them with their main excitation modes.

In Table V, we obtain the relationship between the  $\rho$ - and  $\lambda$ -mode excitations with different color configurations as  $6_\rho < 3_\lambda < 6_\lambda < 3_\rho$  (the number and the subscript represent the color configuration and the excited mode, respectively). For the  $\rho$ -mode  $T_c$  eigenstates, the color configurations of the lower  $|\rho_1^{+/-}\rangle$  state and the higher  $|\rho_2^{+/-}\rangle$  are dominated by  $6_c - \bar{6}_c$  and  $\bar{3}_c - 3_c$  components, respectively. Similar to the S-wave tetraquarks, the  $6_c - \bar{6}_c$  component lies lower than the  $\bar{3}_c - 3_c$  one. In the  $6_c - \bar{6}_c$  configuration, although the interactions in the diquark or antidiquark are repulsive, the potentials between the two clusters are attractive and much stronger than those in the  $\bar{3}_c - 3_c$  one. This leads to a confined  $6_c - \bar{6}_c$  state, which is even lower than the  $\bar{3}_c - 3_c$  one in our quark model.

What is more, as shown in Table V, the mass difference between the lower  $|\rho_1^{+/-}\rangle$  and higher  $|\rho_2^{+/-}\rangle$  is about 300



TABLE IV. The mass spectrum (MeV), the percentage of different color configurations, and the root mean square radius (fm) of the S-wave tetraquark states.

$0^{++}$	Mass	$\bar{3}_c \otimes 3_c$	$6_c \otimes \bar{6}_c$	$1_c \otimes 1_c$	$8_c \otimes 8_c$	$r_{12}/r_{34}$	$r$	$r_{13}/r_{24}$	$r'$
1S	6405	31.9%	68.1%	96.9%	3.13%	0.52	0.31	0.48	0.37
	6498	67.7%	32.3%	5.7%	94.3%	0.51	0.36	0.51	0.36
2S	6867	10.6%	89.4%	80.6%	19.4%	0.65	0.35	0.58	0.46
	7007	89.7%	10.3%	26.0%	74.0%	0.49	0.47	0.59	0.35
$1^{+-}$	Mass	$\bar{3}_c \otimes 3_c$	$6_c \otimes \bar{6}_c$	$1_c \otimes 1_c$	$8_c \otimes 8_c$	$r_{12}/r_{34}$	$r$	$r_{13}/r_{24}$	$r'$
1S	6481	100%	0%	33.3%	66.7%	0.48	0.37	0.51	0.34
2S	6954	100%	0%	33.3%	66.7%	0.61	0.44	0.61	0.43
3S	7024	100%	0%	33.3%	66.7%	0.66	0.42	0.62	0.46
$2^{++}$	Mass	$\bar{3}_c \otimes 3_c$	$6_c \otimes \bar{6}_c$	$1_c \otimes 1_c$	$8_c \otimes 8_c$	$r_{12}/r_{34}$	$r$	$r_{13}/r_{24}$	$r'$
1S	6502	100%	0%	33.3%	66.7%	0.49	0.39	0.53	0.35
2S	6917	100%	0%	33.3%	66.7%	0.55	0.60	0.72	0.39
3S	7030	100%	0%	33.3%	66.7%	0.64	0.46	0.64	0.45

MeV, while that between the two ground  $0^{++}$  S-wave  $T_c$  states is about 100 MeV. This indicates that the mass splittings between the  $6_c - \bar{6}_c$  and  $3_c - \bar{3}_c$   $\rho$ -mode states should be much larger, which is useful to investigate the complicated color configurations in the multi-quark state, especially the rarely known  $6_c - \bar{6}_c$  color configurations.

For the perturbative potentials, we include the spin-orbital and the tensor potentials, which contribute to the mixing of the  $\lambda$ - and  $\rho$ -mode states and shift the mass spectrum. We list the related spin-orbital and tensor factors in Appendix. We display the mass spectra of the P-wave states in Fig. 3 and list the matrices of the Hamiltonian in Table VI. The percentage of the leading eigenstates, and the root mean square radius are also shown in Table VI. The root mean square radii are smaller than 1 fm, which indicates that the four quarks are compactly bound within the tetraquark states.

The spin-orbital and tensor potentials slightly shift the mass spectrum obtained with the leading potentials in Eq. (2). The  $T_c$  state is dominated by one excitation mode except the  $1^{--}$ . The mixing of the two higher  $1^{--}$  modes is large, because the  $|\lambda_3^- \rangle$  state and the  $|\rho_2^- \rangle$  one are nearly accidentally degenerate after considering the perturbative mass shifting. Thus, their mixing is very sensitive to the off-diagonal corrections arising from the spin-orbital and tensor potentials. For the other P-wave  $T_c$ 's, the highest and lightest states are almost totally dominated by  $|\rho_1^{+/-} \rangle$  and  $|\rho_2^{+/-} \rangle$  components, thus, are dominated by the  $6_c - \bar{6}_c$  and  $\bar{3}_c - 3_c$  color configurations, respectively. With the  $6_c - \bar{6}_c$  components, we obtain a quite low-lying  $0^{--}$  state at 6592 MeV. Otherwise, the  $0^{--}$  state should be located at least 300 MeV higher. At the same time, the lowest P-wave state of the other  $T_c$ 's shall almost be a  $\lambda$ -mode excitation. The decay patterns of the lowest states, which are sensitive to the  $\lambda$ - and  $\rho$ -

modes, will be quite different. Thus, one may use the decay patterns of the  $T_c$  states and the mass spectrum of the  $0^{--}$  one to study the  $6_c - \bar{6}_c$  color configurations.

An unavoidable problem of the framework is that the eigenstates are much richer than the experimental data. The reasons are listed as follows. First, in the calculation, we have to solve the Schrödinger equation with finite numbers of basis in the calculation, which indicates a finite volume of space. Some of the eigenstates might be the discretized scattering states instead of a real resonance. Second, some resonances have large decay widths and their signals might be overwhelmed by the background in some specific channels and are hard to be observed in experiments. What is more, a broad structure, for instance, the one ranging from 6.2 – 6.8 GeV in LHCb may be a broad resonance or sometimes a mixture of several states. To exclude the redundant states and understand the inner structures of the resonances in experiments, we need to corroborate the complex scaling method and calculate decay widths in the future.

## V. POSSIBLE DECAY MODES

For a  $T_c$  state, its decay modes include  $T_c \rightarrow (c\bar{c}) + (c\bar{c})$ ,  $D^{(*)}\bar{D}^{(*)}$ , light hadrons or  $\gamma\gamma$ , etc. It locates above the threshold of two charmonia, the fall-apart decays  $T_c \rightarrow (c\bar{c}) + (c\bar{c})$  are therefore dominant. We have listed some possible low-lying two-charmonium channels in Table VII.

The S-wave radially excited states are much higher than the low-lying di- $\eta_c$ ,  $J/\psi\eta_c$ , or di- $J/\psi$  channels. They will decay into these channels with a large phase space and might be broad. The P-wave  $T_c$  states will decay into the lowest two-charmonium channels di- $\eta_c$ ,

TABLE V. The mass spectrum (MeV) and the percentages of different color configurations in the P-wave  $T_c$  states obtained with leading potentials, including the Coulomb, linear confinement and hyperfine potentials in Eq. (2). The eigenstates are labeled by  $|\rho/\lambda_i^C\rangle$ , where  $C$  is the C-parity and  $i = 1, 2, 3$  represent different states in the ascending order of the mass.

$J^{-+}$	Mass	$ 3_\lambda^+; {}^3P_{0,1,2}\rangle$	$ 3_\rho^+; {}^3P_{0,1,2}\rangle$	$ 6_\rho^+; {}^3P_{0,1,2}\rangle$	$1_c \otimes 1_c$	$8_c \otimes 8_c$	$6_\rho^+ < 3_\lambda^+ < 3_\rho^+$
$ \lambda_1^+\rangle$	6746	99.5%	0.4%	0.1%	33.4%	66.6%	
$J^{-+}$	Mass	$ 3_\lambda^+; {}^3P_{0,1,2}\rangle$	$ 3_\rho^+; {}^3P_{0,1,2}\rangle$	$ 6_\rho^+; {}^3P_{0,1,2}\rangle$	$1_c \otimes 1_c$	$8_c \otimes 8_c$	
$ \rho_1^+\rangle$	6599	0.1%	24.5%	75.4%	58.5%	41.5%	
$ \rho_2^+\rangle$	6894	0.5%	72.0%	27.5%	42.5%	57.5%	$6_\rho^- < 3_\lambda^- < 6_\lambda^- < 3_\rho^-$
$J^{--}$	Mass	$ 3_\lambda^-; {}^1P_1\rangle$	$ 6_\lambda^-; {}^1P_1\rangle$	$ 3_\lambda^-; {}^5P_{1,2,3}\rangle$	$1_c \otimes 1_c$	$8_c \otimes 8_c$	
$ \lambda_1^-\rangle$	6740	98.9%	1.1%	0%	33.7%	66.3%	
$ \lambda_2^-\rangle$	6741	0%	0%	100%	33.3%	66.7%	
$ \lambda_3^-\rangle$	6885	1.4%	98.6%	0%	66.2%	33.8%	$6_\rho^- < 3_\lambda^- < 6_\lambda^- < 3_\rho^-$
$J^{--}$	Mass	$ 3_\rho^-; {}^3P_{0,1,2}\rangle$	$ 6_\rho^-; {}^3P_{0,1,2}\rangle$		$1_c \otimes 1_c$	$8_c \otimes 8_c$	
$ \rho_1^-\rangle$	6561	27.1%	72.9%		57.6%	42.4%	
$ \rho_2^-\rangle$	6913	72.1%	27.9%		42.6%	57.4%	

TABLE VI. The mass spectrum (MeV), the percentages of different  $\lambda$ - and  $\rho$ -mode components, and the root mean square radius (fm) of the P-wave tetraquark states. In the second row, we display the mass spectrum obtained with the leading potentials in Eq. (2) and the mass corrections from the perturbative spin-orbital and tensor interactions in the mass matrix.

$J^{PC}$		Mass	$ \lambda_1^{+/-}\rangle$	$ \lambda_2^-\rangle$	$ \lambda_3^-\rangle$	$ \rho_1^{+/-}\rangle$	$ \rho_2^{+/-}\rangle$	$r_{12}/r_{34}$	$r$	$r_{13}/r_{24}$	$r'$
$0^{-+}$	$\begin{pmatrix} 6746-20 & -20 & -34 \\ -20 & 6599+2 & -42 \\ -34 & -42 & 6894-62 \end{pmatrix}$	6589	3.5%			92.8%	3.7%	0.62	0.33	0.60	0.50
		6723	90.4%			5.2%	4.4%	0.52	0.43	0.66	0.37
		6847	6.0%			2.1%	91.9%	0.57	0.38	0.61	0.47
$0^{--}$	$\begin{pmatrix} 6561+31 & -11 \\ -11 & 6913-14 \end{pmatrix}$	6592				99.9%	0.1%	0.61	0.32	0.59	0.49
		6899				0.1%	99.9%	0.58	0.38	0.61	0.48
$1^{-+}$	$\begin{pmatrix} 6746-3 & -4 & -6 \\ -4 & 6599+9 & 8 \\ -6 & 8 & 6894-10 \end{pmatrix}$	6608	0.1%			99.8%	0.1%	0.63	0.33	0.60	0.50
		6743	99.7%			0.1%	0.2%	0.51	0.43	0.66	0.36
		6884	0.2%			0.1%	99.7%	0.57	0.37	0.60	0.47
$1^{--}$	$\begin{pmatrix} 6740 & -2 & 0 & -10 & 9 \\ -2 & 6741-23 & 7 & -19 & 26 \\ 0 & 7 & 6885 & -2 & -25 \\ -10 & -19 & -2 & 6561-1 & 21 \\ 9 & 26 & -25 & 21 & 6913-28 \end{pmatrix}$	6555	0.3%	1.6%	$\sim 0\%$	97.5%	0.6%	0.61	0.32	0.59	0.49
		6716	0.6%	94.8%	0.4%	2.0%	2.1%	0.52	0.42	0.65	0.37
		6740	98.8%	0.9%	$\sim 0\%$	0.2%	0.1%	0.51	0.43	0.65	0.36
		6864	0.2%	2.2%	55.7%	0.1%	41.9%	0.62	0.35	0.64	0.47
		6911	0.1%	0.5%	43.9%	0.2%	55.3%	0.61	0.36	0.63	0.47
$2^{-+}$	$\begin{pmatrix} 6746+6 & 7 & 10 \\ 7 & 6599-6 & 13 \\ 10 & 13 & 6894+18 \end{pmatrix}$	6592	0.2%			99.7%	0.1%	0.63	0.33	0.60	0.50
		6752	99.4%			0.2%	0.4%	0.52	0.43	0.66	0.36
		6913	0.4%			0.2%	99.4%	0.57	0.38	0.60	0.47
$2^{--}$	$\begin{pmatrix} 6741-2 & 7 & -9 \\ 7 & 6561-6 & -15 \\ -9 & -15 & 6913+20 \end{pmatrix}$	6554		0.1%		99.7%	0.2%	0.61	0.32	0.59	0.49
		6739		99.6%		0.1%	0.2%	0.51	0.43	0.66	0.36
		6934		0.2%		0.2%	99.6%	0.57	0.38	0.61	0.48
$3^{--}$	6741+11	6753		100%				0.51	0.43	0.66	0.36

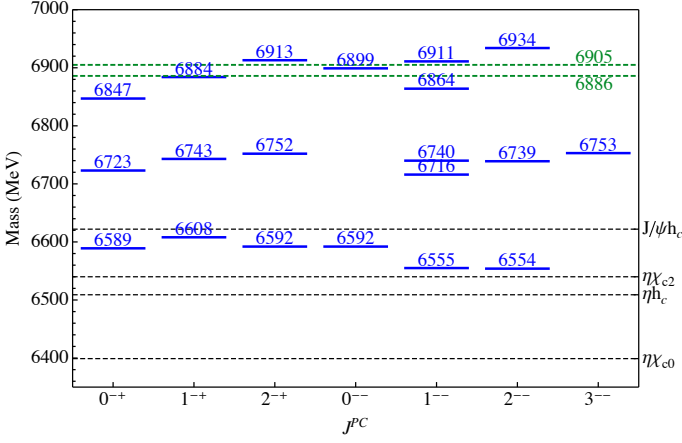


FIG. 3. The mass spectrum of the P-wave  $T_c$  states. The green dashed lines stand for the two fitted central mass values of the  $X(6900)$  given by experiments [38].

$\eta_c J/\psi$ , or di- $J/\psi$  with a P-wave orbital excitation. These decays are kinematically suppressed at  $\mathcal{O}(p^3)$  ( $p$  is the relative momentum in the final state). Their S-wave decays modes are the two-charmonium channels composed of a P-wave charmonium and an S-wave one. For the low-lying P-wave  $T_c$  states, the S-wave decay modes are suppressed or even not allowed due to the small phase space. Thus, they may be narrow. For the  $0^{--}$  and  $1^{--}$   $T_c$  states, their lowest possible decay modes are the P-wave  $\eta_c J/\psi$  channel and di- $J/\psi$  channel, respectively. These exotic  $J^{PC}$  quantum numbers are not allowed in the conventional charmonium sector. The search of the above channels will help to enrich the hadronic spectrum.

For the di- $J/\psi$  decay mode, the possible  $J^{PC}$  quantum numbers are  $0^{++}$  and  $2^{++}$  for the S-wave states, while those are  $0^{--}$ ,  $1^{--}$ , and  $2^{--}$  for the P-wave states. Based on the mass spectra, the first radial excitations with the masses  $M(0^{++}) = 6867$  MeV and  $M(2^{++}) = 6917$  MeV, or the  $1^{--}$  and  $2^{--}$  P-wave states with the masses  $M(1^{--}) = 6884$  MeV and  $M(2^{--}) = 6913$  MeV, may be the candidates for the  $X(6900)$ . As an S-wave radial excitation, it will decay into the S-wave di- $\eta_c$  or di- $J/\psi$  channels. As a P-wave  $T_c$  state, its decays into the two final states are kinetically suppressed. The other S-wave decay modes are  $J/\psi h_c$  for the  $1^{--}$   $T_c$  state,  $\eta_c \chi_{c2}$  and  $J/\psi h_c$  for the  $2^{--}$  one with smaller phase space. Thus, the  $X(6900)$  as an S-wave  $T_c$  state should be much broader. We can determine the  $J^{PC}$  quantum numbers of the  $X(6900)$  by studying their decay patterns in the future.

## VI. DISCUSSIONS

In Sec. IV, we obtain the relation among the P-wave  $\rho$ -mode and  $\lambda$ -mode excitations with different color configurations,  $6_\rho < 3_\lambda < 6_\lambda < 3_\rho$ . Moreover, if we compare the mass spectra of the S-wave and P-wave  $T_c$  states as

illustrated in Fig. 2 and Fig. 3, the mass gaps are much smaller than those of the charmonia. In this section, we will give a qualitative discussion about the two results.

In the baryon sector, if the confinement potential dominates the binding, one can use a phenomenological harmonic oscillator potential to discuss the feature of the two excitation modes for the P-wave baryons [93]. We expand the method to discuss the  $T_c$  state.

For the  $3_c - \bar{3}_c$  confined  $T_c$  state, the Hamiltonian in the harmonic oscillator potential is written as

$$H = \sum_{i=1}^4 \frac{\mathbf{p}_i^2}{2m_i} + \frac{k}{2}(r_{12}^2 + r_{34}^2) + \frac{k'}{4}(r_{13}^2 + r_{24}^2 + r_{14}^2 + r_{23}^2) \\ = \frac{\mathbf{p}_a^2}{2u_a} + \frac{\mathbf{p}_b^2}{2u_b} + \frac{\mathbf{p}_{ab}^2}{2u_{ab}} + \frac{u_a \omega_a^2}{2} r_{12}^2 + \frac{u_b \omega_b^2}{2} r_{34}^2 + \frac{u_{ab} \omega_{ab}^2}{2} r^2, \quad (9)$$

where  $\mathbf{p}_{a/b/ab}$  and  $u_{a/b/ab}$  are the relative momenta and the reduced masses of the diquark/antidiquarks, or those between the two clusters.  $k$  and  $k'$  are the coefficients of the confinement potential. The frequencies  $\omega$  are given by

$$\omega_a = \sqrt{\frac{2k + k'}{2u_a}}, \quad \omega_b = \sqrt{\frac{2k + k'}{2u_b}}, \quad \omega_{ab} = \sqrt{\frac{2k'}{u_{ab}}}. \quad (10)$$

The eigenvalue then reads

$$E = (2n_a + l_a + 3/2)\hbar\omega_a + (2n_b + l_b + 3/2)\hbar\omega_b \\ + (2n_{ab} + l_{ab} + 3/2)\hbar\omega_{ab}. \quad (11)$$

For the fully heavy tetraquark state  $QQ\bar{Q}\bar{Q}$ , one has  $u_a = u_b = \frac{m_Q}{2}$  and  $u_{ab} = m_Q$ . The coupling constant  $k$  and  $k'$  should be similar to each other according to the experiences in the conventional hadrons. If we assume  $k = k'$ , one has

$$\omega_a = \omega_b = \sqrt{\frac{3k}{m_Q}} > \omega_{ab} = \sqrt{\frac{2k}{m_Q}}, \quad (12)$$

which indicates that the  $3_\lambda$  mode P-wave state is located lower than the  $3_\rho$  mode ones. This is also a feature of the P-wave baryons [93].

For the  $6_c - \bar{6}_c$  state, we can write the Hamiltonian similarly,

$$H = \sum_i \frac{\mathbf{p}_i^2}{2m_i} - \frac{k}{4}(r_{12}^2 + r_{34}^2) + \frac{5k'}{8}(r_{13}^2 + r_{24}^2 + r_{14}^2 + r_{23}^2) \\ = \frac{\mathbf{p}_a^2}{2u_a} + \frac{\mathbf{p}_b^2}{2u_b} + \frac{\mathbf{p}_{ab}^2}{2u_{ab}} - \frac{u_a \omega_a^2}{2} r_{12}^2 - \frac{u_b \omega_b^2}{2} r_{34}^2 + \frac{u_{ab} \omega_{ab}^2}{2} r^2, \quad (13)$$

with the frequencies as

$$\omega_a = \sqrt{\frac{-2k + 5k'}{4u_a}}, \quad \omega_b = \sqrt{\frac{-2k + 5k'}{4u_b}}, \quad \omega_{ab} = \sqrt{\frac{5k'}{u_{ab}}}. \quad (14)$$



TABLE VII. The possible decay modes of the  $T_c$  states. We use the bold font to emphasize the  $J/\psi J/\psi$  mode, where the  $X(6900)$  was observed [38].

$J^{PC}$	Decay modes
$0^{++}$	$\eta_c \eta_c$ , <b><math>J/\psi J/\psi</math></b> , $\chi_{c1} \eta_c$ (P-wave), $J/\psi h_c(1P)$ (P-wave), $J/\psi \psi(2S)$ , $\chi_{c0} \chi_{c0}$
$1^{+-}$	$\eta_c J/\psi$ , $h_c \eta_c$ (P-wave), $J/\psi \chi_{c1}$ (P-wave), $\eta_c \psi'$ , $h_c \chi_{c0}$
$2^{++}$	<b><math>J/\psi J/\psi</math></b> , $\eta_c \chi_{c1}$ (P-wave), $\eta_c \chi_{c2}$ (P-wave), $J/\psi h_c$ (P-wave), $J/\psi \psi(2S)$ , $\chi_{c0} \chi_{c2}$
$0^{-+}$	<b><math>J/\psi J/\psi</math></b> (P-wave), $\eta_c \chi_{c0}$ , $J/\psi h_c$ , $J/\psi \psi(2S)$ (P-wave)
$1^{-+}$	<b><math>J/\psi J/\psi</math></b> (P-wave) $J/\psi h_c$ , $J/\psi \psi(2S)$ (P-wave)
$2^{-+}$	<b><math>J/\psi J/\psi</math></b> (P-wave), $\eta_c \chi_{c2}$ , $J/\psi h_c$ , $J/\psi \psi(2S)$ (P-wave)
$0^{--}$	$\eta_c J/\psi$ (P-wave), $J/\psi \chi_{c1}$ , $\eta_c \psi(2S)$ (P-wave)
$1^{--}$	$\eta_c J/\psi$ (P-wave), $\eta_c h_c$ , $J/\psi \chi_{c0}$ , $J/\psi \chi_{c1}$ , $J/\psi \chi_{c2}$ , $\eta_c \psi'$ (P-wave)
$2^{--}$	$\eta_c J/\psi$ (P-wave), $J/\psi \chi_{c1}$ , $J/\psi \chi_{c2}$ , $\eta_c \psi'$ (P-wave), $h_c \chi_{c0}$ (P-wave)
$3^{--}$	$J/\psi \chi_{c2}$

If  $k = k'$ , one obtains

$$\omega_a = \omega_b = \sqrt{\frac{3k}{2m_Q}} < \omega_{ab} = \sqrt{\frac{5k}{m_Q}}, \quad (15)$$

which indicates that the  $6_\lambda$  mode state is located higher than the  $6_\rho$  mode one.

With Eq. (12) and Eq. (15), we obtain the qualitative relationship among the mass spectra

$$6_\rho < 3_\lambda < 3_\rho < 6_\lambda. \quad (16)$$

This is consistent with the relation in Table V except that the  $3_\rho$  is lower than the  $6_\lambda$ , where the relation is inverse in the dynamical calculations.

We can also write the Hamiltonian of the heavy quarkonium in the harmonic oscillator potential as follows:

$$H = \sum_i \frac{p_i^2}{2m_i} + kr_{12}^2 = \frac{p^2}{2u_m} + \frac{u_m \omega^2}{2} r_{12}^2, \quad (17)$$

with

$$u_m = \frac{m_Q}{2}, \quad \omega_m = \sqrt{\frac{4k}{m_Q}}, \quad (18)$$

where  $u_m$  and  $\omega_m$  are the reduced mass and the frequency of the charmonium, respectively. In general, the mass splitting for the ground S-wave and P-wave charmonium  $\hbar\sqrt{\frac{4k}{m_c}}$  is about 400 ~ 500 MeV. In contrast, the mass splitting for the ground S-wave and P-wave  $T_c$  state is  $\hbar\sqrt{\frac{3k}{2m_c}}$  and its value is about 245 ~ 300 MeV. Thus, the small mass difference for the S-wave and P-wave  $T_c$  state arises from the low-lying  $6_\rho$  component.

## VII. SUMMARY

In this work, we have systematically calculated the mass spectra of the S-wave and P-wave  $T_c$  states and discussed their structures with a nonrelativistic quark model. The parameters are determined by the spectrum of the charmonium. In the calculation, we treat the OGE Coulomb-like, linear confinement, and hyperfine interactions as leading order potentials. The remaining spin-orbital and tensor potentials are treated as the perturbative interactions, which will contribute to the mass shifts.

In the analysis of the  $T_c$  wave function, we include both the  $\bar{3}_c - 3_c$  and the  $6_c - \bar{6}_c$  color configurations. To obtain the mass spectrum, we solve the Schrödinger equation with the variational method. For the S-wave  $T_c$  states, we do not consider the perturbative potentials since the induced mass shifts should be much smaller than the mass differences arising from the leading potentials and will not influence the mass spectrum significantly. For the P-wave state, the spin-orbital and tensor potentials are essential to distinguish the  $T_c$  states with different  $J^{PC}$  quantum numbers. Their contributions are calculated in the basis of the eigenvectors which are obtained with only the leading potentials. We give the numerical results for the S-wave  $T_c$  states plus their radial excitations, and the P-wave  $T_c$  states in Fig. 2 and Fig. 3, respectively.

For the S-wave state, we find that the ground state is located above the low-lying two-charmonium channels di- $\eta_c$ ,  $J/\psi \eta_c$  and di- $J/\psi$ . The  $6_c - \bar{6}_c$  color configuration only appears in the  $0^{++}$  state and dominates the ground state as illustrated in Table IV. In other words, the  $6_c - \bar{6}_c$  component is located lower than the  $\bar{3}_c - 3_c$  one, because the prior one has an attractive and much stronger interactions between the diquark and antidiquark. The fall-apart decays of the S-wave  $T_c$  states into two charmonia

imply that these states, especially their radial excitations might be very broad. For the  $X(6900)$  state, the ground states are located much lower, while the first radial excitation of the  $0^{++}$  and  $2^{++}$  state lie very close. If it turns out to be the first radial excitation, it shall have a broad decay width.

For the P-wave state, we focus on two excited modes, i.e., the  $\lambda$ -mode and  $\rho$ -mode, and their properties. The two excitation modes with the negative charge parity do not couple with each other, while the modes with the positive C-parity mix quite slightly because of the hyperfine potential. The relation among different modes with different color configurations is  $6_\rho < 3_\lambda < 6_\lambda < 3_\rho$ . At the next order, the spin-orbital and tensor potentials cause the small mass shifting and their mixing. Almost all of the mixing is small and one mode is dominant as illustrated in Table VI. The mass spectrum of the P-wave  $\rho$ -mode  $T_c$  state is quite sensitive to the color configurations, which is useful to investigate the role of the rare  $6_c - \bar{6}_c$  color configuration in the multi-quark system. Moreover, the small mass gap between the P-wave and the ground S-wave  $T_c$  states is due to low-lying  $\rho$ -mode excitations with the  $6_c - \bar{6}_c$  color configuration. The masses of the  $1^{-+}$  and  $2^{-+}$  tetraquarks are 6884 MeV and 6913 MeV, respectively, which is consistent with the mass of the  $X(6900)$  state. If we treat it as a P-wave  $T_c$  state, as illustrated in Table VII, its decays into the lowing state are kinematically suppressed. Its S-wave decay modes contain an excited P-wave charmonium and have a small phase space. Thus, the decay width of the P-wave tetraquarks are expected to be narrower than the S-wave ones. More studies of the decay patterns will be useful to determine its  $J^{PC}$  quantum numbers. Besides  $X(6900)$ , there may exist many other tetraquark states. The  $T_c$  states with the  $J^{PC} = 0^{--}$  and  $1^{-+}$  are of special interest since they are not allowed in the conventional quark model. The lowest states are narrow and the phase-space-allowed decay modes are the P-wave  $\eta_c J/\psi$  and di- $J/\psi$  channels, respectively. If observed, they are unambiguously the multi-quark system, which will enrich the hadron spectroscopy. Hopefully, our calculations will be useful for the search of the new exotic tetraquark states. More experimental and theo-

retical works are expected to verify and understand the multi-quark system in the future.

### Appendix A: The spin, spin-orbital and tensor factors

In this section, we present the related color magnetic factors in Table VIII. To calculate the spin factors, we extract the spin wave functions of different color-flavor configurations listed in Table III. For the  $J^{PC} = 0^{-+}$ ,  $1^{-+}$ ,  $2^{-+}$  states, the spin wave function of the  $\lambda$ -mode is

$$\chi_s^\lambda = [[QQ]_{\bar{3}_c}^1 [\bar{Q}_2 \bar{Q}_3]_{\bar{3}_c}^1]_{1_c}^1. \quad (A1)$$

The spin wave function of the two  $\rho$ -mode excitations read,

$$\begin{aligned} [[QQ]_{\bar{3}_c}^0, \rho]_{\bar{3}_c}^1 [\bar{Q}\bar{Q}]_{\bar{3}_c}^1 &: \chi_{s1}^\rho = ([QQ]_{\bar{3}_c}^0 [\bar{Q}\bar{Q}]_{\bar{3}_c}^1)^1, \\ [[QQ]_{\bar{6}_c}^1, \rho]_{\bar{6}_c}^0 [\bar{Q}\bar{Q}]_{\bar{6}_c}^0 &: \chi_{s2}^\rho = ([QQ]_{\bar{6}_c}^1 [\bar{Q}\bar{Q}]_{\bar{6}_c}^0)^1. \end{aligned} \quad (A2)$$

Here, we select the spin wave functions for the the color-flavor-spin configurations with the P-wave excitation in the diquark as an example. The corresponding color magnetic factors are listed in Table VIII. The P-wave may also appear in the antidiquark. The calculation of their factors is similar.

The spin-orbital plus the tensor factors are listed in Table IX- Table XI.

### ACKNOWLEDGMENTS

We are grateful for the helpful discussions with Xin-Zhen Weng. This project was supported by the National Natural Science Foundation of China (11975033 and 12070131001). M. Oka is supported in part by the JSPS KAKENHI (Nos. 19H05159, 20K03959, and 21H00132). G.J. Wang was supported by JSPS KAKENHI (No. 20F20026). L. Meng was funded by the Deutsche Forschungsgemeinschaft (DFG, German Research Foundation, Project ID 196253076-TRR 110).

- 
- [1] N. Brambilla, S. Eidelman, C. Hanhart, A. Nefediev, C.-P. Shen, C. E. Thomas, A. Vairo, and C.-Z. Yuan, *Phys. Rept.* **873**, 1 (2020), [arXiv:1907.07583 \[hep-ex\]](#).
  - [2] H.-X. Chen, W. Chen, X. Liu, and S.-L. Zhu, *Phys. Rept.* **639**, 1 (2016), [arXiv:1601.02092 \[hep-ph\]](#).
  - [3] F.-K. Guo, C. Hanhart, U.-G. Meißner, Q. Wang, Q. Zhao, and B.-S. Zou, *Rev. Mod. Phys.* **90**, 015004 (2018), [arXiv:1705.00141 \[hep-ph\]](#).
  - [4] A. Esposito, A. Pilloni, and A. D. Polosa, *Phys. Rept.* **668**, 1 (2017), [arXiv:1611.07920 \[hep-ph\]](#).
  - [5] A. Hosaka, T. Iijima, K. Miyabayashi, Y. Sakai, and S. Yasui, *PTEP* **2016**, 062C01 (2016), [arXiv:1603.09229 \[hep-ph\]](#).

- [6] A. Ali, J. S. Lange, and S. Stone, *Prog. Part. Nucl. Phys.* **97**, 123 (2017), [arXiv:1706.00610 \[hep-ph\]](#).
- [7] Y.-R. Liu, H.-X. Chen, W. Chen, X. Liu, and S.-L. Zhu, *Prog. Part. Nucl. Phys.* **107**, 237 (2019), [arXiv:1903.11976 \[hep-ph\]](#).
- [8] R. F. Lebed, R. E. Mitchell, and E. S. Swanson, *Prog. Part. Nucl. Phys.* **93**, 143 (2017), [arXiv:1610.04528 \[hep-ph\]](#).
- [9] L. Meng, B. Wang, G.-J. Wang, and S.-L. Zhu, *Phys. Rev. D* **100**, 014031 (2019), [arXiv:1905.04113 \[hep-ph\]](#).
- [10] B. Wang, L. Meng, and S.-L. Zhu, *JHEP* **11**, 108 (2019), [arXiv:1905.04113 \[hep-ph\]](#).

TABLE VIII. The color magnetic factors  $\langle H_{CM}^{ij} = \frac{\lambda_i}{2} \cdot \frac{\lambda_j}{2} s_i \cdot s_j \rangle$  for a fully heavy tetraquark state  $Q_1 Q_2 \bar{Q}_3 \bar{Q}_4$ .

	$\langle H_{CM}^{Q_1 \bar{Q}_3} \rangle$	$\langle H_{CM}^{Q_2 \bar{Q}_4} \rangle$	$\langle H_{CM}^{Q_1 \bar{Q}_4} \rangle$	$\langle H_{CM}^{Q_2 \bar{Q}_3} \rangle$	$\langle H_{CM}^{Q_1 Q_2} \rangle$	$\langle H_{CM}^{\bar{Q}_3 \bar{Q}_4} \rangle$
$\langle \chi_s^\lambda   H_{CM}^{ij}   \chi_s^\lambda \rangle$	$\frac{1}{12}$	$\frac{1}{12}$	$\frac{1}{12}$	$\frac{1}{12}$	$-\frac{1}{6}$	$-\frac{1}{6}$
$\langle \chi_{s1}^\rho   H_{CM}^{ij}   \chi_{s1}^\rho \rangle$	0	0	0	0	$\frac{1}{2}$	$-\frac{1}{6}$
$\langle \chi_{s2}^\rho   H_{CM}^{ij}   \chi_{s2}^\rho \rangle$	0	0	0	0	$\frac{1}{12}$	$-\frac{1}{4}$
$\langle \chi_s^\lambda   H_{CM}^{ij}   \chi_{s1}^\rho \rangle$	$\frac{1}{6\sqrt{2}}$	$-\frac{1}{6\sqrt{2}}$	$\frac{1}{6\sqrt{2}}$	$-\frac{1}{6\sqrt{2}}$	0	0
$\langle \chi_s^\lambda   H_{CM}^{ij}   \chi_{s2}^\rho \rangle$	$-\frac{1}{4}$	$\frac{1}{4}$	$-\frac{1}{4}$	$\frac{1}{4}$	0	0
$\langle \chi_{s1}^\rho   H_{CM}^{ij}   \chi_{s2}^\rho \rangle$	$-\frac{1}{4\sqrt{2}}$	$-\frac{1}{4\sqrt{2}}$	$-\frac{1}{4\sqrt{2}}$	$-\frac{1}{4\sqrt{2}}$	0	0

TABLE IX. The spin-orbital and tensor factors for the  $\lambda$ -mode P-wave states.

$J^{PC}$			$J$	$Q_1 Q_2 \bar{Q}_3 \bar{Q}_4$	$Q_1 \bar{Q}_3 Q_2 \bar{Q}_4$	$Q_1 \bar{Q}_4 Q_2 \bar{Q}_3$			
$J^{-+}$	$[[[QQ]_{\bar{3}_c}^1 [\bar{Q}\bar{Q}]_{3_c}^1, \lambda]^J]$	$\mathbf{L}_{ij} \cdot \mathbf{S}_{ij}$	$J = 0$	0	0	-1	-1	-1	-1
			$J = 1$	0	0	$-\frac{1}{2}$	$-\frac{1}{2}$	$-\frac{1}{2}$	$-\frac{1}{2}$
			$J = 2$	0	0	$\frac{1}{2}$	$\frac{1}{2}$	$\frac{1}{2}$	$\frac{1}{2}$
		$\mathcal{S}_{ij}$	$J = 0$	0	0	$-\frac{1}{2}$	$-\frac{1}{2}$	$-\frac{1}{2}$	$-\frac{1}{2}$
			$J = 1$	0	0	$\frac{1}{4}$	$\frac{1}{4}$	$\frac{1}{4}$	$\frac{1}{4}$
			$J = 2$	0	0	$-\frac{1}{20}$	$-\frac{1}{20}$	$-\frac{1}{20}$	$-\frac{1}{20}$
$1^{--}$	$\phi_1(^1P_1) = [[[[QQ]_{\bar{3}_c}^1 [\bar{Q}\bar{Q}]_{3_c}^1]_{1_c}^0, \lambda]_{1_c}^1]$	$\mathbf{L}_{ij} \cdot \mathbf{S}_{ij}$	$\langle \phi_1(^1P_1)   \hat{O}   \phi_1(^1P_1) \rangle$	0	0	0	0	0	0
			$\langle \phi_2(^1P_1)   \hat{O}   \phi_2(^1P_1) \rangle$	0	0	0	0	0	0
			$\langle \phi_3(^5P_1)   \hat{O}   \phi_3(^5P_1) \rangle$	0	0	$-\frac{3}{2}$	$-\frac{3}{2}$	$-\frac{3}{2}$	$-\frac{3}{2}$
			$\langle \phi_1(^1P_1)   \hat{O}   \phi_2(^1P_1) \rangle$	0	0	0	0	0	0
			$\langle \phi_1(^1P_1)   \hat{O}   \phi_3(^5P_1) \rangle$	0	0	0	0	0	0
			$\langle \phi_2(^1P_1)   \hat{O}   \phi_3(^5P_1) \rangle$	0	0	0	0	0	0
	$\phi_2(^1P_1) = [[[[QQ]_{6_c}^0 [\bar{Q}\bar{Q}]_{6_c}^0]_{1_c}^0, \lambda]_{1_c}^1]$	$\mathcal{S}_{ij}$	$\langle \phi_1(^1P_1)   \hat{O}   \phi_1(^1P_1) \rangle$	0	0	0	0	0	0
			$\langle \phi_2(^1P_1)   \hat{O}   \phi_2(^1P_1) \rangle$	0	0	0	0	0	0
			$\langle \phi_3(^5P_1)   \hat{O}   \phi_3(^5P_1) \rangle$	0	0	$-\frac{7}{20}$	$-\frac{7}{20}$	$-\frac{7}{20}$	$-\frac{7}{20}$
			$\langle \phi_1(^1P_1)   \hat{O}   \phi_2(^1P_1) \rangle$	0	0	0	0	0	0
			$\langle \phi_1(^1P_1)   \hat{O}   \phi_3(^5P_1) \rangle$	0	0	$\frac{1}{2\sqrt{5}}$	$\frac{1}{2\sqrt{5}}$	$\frac{1}{2\sqrt{5}}$	$\frac{1}{2\sqrt{5}}$
			$\langle \phi_2(^1P_1)   \hat{O}   \phi_3(^5P_1) \rangle$	0	0	$-\frac{\sqrt{\frac{3}{2}}}{2}$	$-\frac{\sqrt{\frac{3}{2}}}{2}$	$\frac{\sqrt{\frac{3}{2}}}{2}$	$\frac{\sqrt{\frac{3}{2}}}{2}$
$2^{--}$	$[[[[QQ]_{\bar{3}_c}^1 [\bar{Q}\bar{Q}]_{3_c}^1]_{1_c}^2, \lambda]_{1_c}^2]$	$\mathbf{L}_{ij} \cdot \mathbf{S}_{ij}$	$\langle \phi_1(^5P_2)   \hat{O}   \phi_1(^5P_2) \rangle$	0	0	$-\frac{1}{2}$	$-\frac{1}{2}$	$-\frac{1}{2}$	$-\frac{1}{2}$
		$\mathcal{S}_{ij}$		0	0	$\frac{7}{20}$	$\frac{7}{20}$	$\frac{7}{20}$	$\frac{7}{20}$
$3^{--}$	$[[[[QQ]_{\bar{3}_c}^1 [\bar{Q}\bar{Q}]_{3_c}^1]_{1_c}^2, \lambda]_{1_c}^3]$	$\mathbf{L}_{ij} \cdot \mathbf{S}_{ij}$	$\langle \phi_1(^5P_3)   \hat{O}   \phi_1(^5P_3) \rangle$	0	0	1	1	1	1
		$\mathcal{S}_{ij}$		0	0	$-\frac{1}{10}$	$-\frac{1}{10}$	$-\frac{1}{10}$	$-\frac{1}{10}$

TABLE X. The spin-orbital and tensor factors of the  $\rho$ -mode P-wave states. The position of the matrix elements corresponds to the subscripts of the color-flavor-spin configurations.

[illegible]

TABLE XI. The spin-orbital and tensor factors for the mixing of the  $\lambda$ -mode and  $\rho$ -mode P-wave states. For conciseness, we list the unit for each subregion in the table and the factor is the product of the unit and  $0, \pm 1$ .

$J^{PC}$		$\mathbf{L}_{ij} \cdot \mathbf{S}_{ij}$	$\mathcal{S}_{ij}$
		$Q_1\bar{Q}_2 \quad \bar{Q}_3\bar{Q}_4 \quad Q_1\bar{Q}_3 \quad Q_2\bar{Q}_4 \quad Q_1\bar{Q}_4 \quad Q_2\bar{Q}_3$	$Q_1\bar{Q}_2 \quad \bar{Q}_3\bar{Q}_4 \quad Q_1\bar{Q}_3 \quad Q_2\bar{Q}_4 \quad Q_1\bar{Q}_4 \quad Q_2\bar{Q}_3$
$0^{-+}$	$[[[QQ]_{\frac{3}{2}}^0, \rho]_{\frac{3}{2}}^1 [\bar{Q}\bar{Q}]_{\frac{3}{2}}^1]_{1_c}^0$	$[[[QQ]_{\frac{3}{2}}^1 [\bar{Q}\bar{Q}]_{\frac{3}{2}}^1]_{1_c}^0, \lambda]_{1_c}^0$ (unit of $\frac{1}{\sqrt{2}}$ )	$[[[QQ]_{\frac{3}{2}}^1 [\bar{Q}\bar{Q}]_{\frac{3}{2}}^1]_{1_c}^0, \lambda]_{1_c}^0$ (unit of $\frac{1}{2\sqrt{2}}$ )
	$[[[QQ]_{\frac{3}{2}}^1 [\bar{Q}\bar{Q}]_{\frac{3}{2}}^0, \rho]_{\frac{3}{2}}^1]_{1_c}^0$	0 0 1 -1 1 -1	0 0 1 -1 1 -1
	$[[[QQ]_{\frac{3}{2}}^1 [\bar{Q}\bar{Q}]_{\frac{3}{2}}^0, \rho]_{\frac{3}{2}}^1]_{1_c}^0$	0 0 -1 1 1 -1	0 0 -1 1 1 -1
	$[[[QQ]_{\frac{3}{2}}^1 [\bar{Q}\bar{Q}]_{\frac{3}{2}}^0, \rho]_{\frac{3}{2}}^1]_{1_c}^0$	0 0 -1 1 1 -1	0 0 -1 1 1 -1
	$[[[QQ]_{\frac{3}{2}}^1 [\bar{Q}\bar{Q}]_{\frac{3}{2}}^0, \rho]_{\frac{3}{2}}^1]_{1_c}^0$	0 0 1 -1 1 -1	0 0 1 -1 1 -1
$1^{-+}$	$[[[QQ]_{\frac{3}{2}}^0, \rho]_{\frac{3}{2}}^1 [\bar{Q}\bar{Q}]_{\frac{3}{2}}^1]_{1_c}^1$	$[[[QQ]_{\frac{3}{2}}^1 [\bar{Q}\bar{Q}]_{\frac{3}{2}}^1]_{1_c}^1, \lambda]_{1_c}^1$ (unit of $\frac{1}{2\sqrt{2}}$ )	$[[[QQ]_{\frac{3}{2}}^1 [\bar{Q}\bar{Q}]_{\frac{3}{2}}^1]_{1_c}^1, \lambda]_{1_c}^1$ (unit of $\frac{1}{4\sqrt{2}}$ )
	$[[[QQ]_{\frac{3}{2}}^1 [\bar{Q}\bar{Q}]_{\frac{3}{2}}^0, \rho]_{\frac{3}{2}}^1]_{1_c}^1$	0 0 1 -1 1 -1	0 0 -1 1 -1 1
	$[[[QQ]_{\frac{3}{2}}^1 [\bar{Q}\bar{Q}]_{\frac{3}{2}}^0, \rho]_{\frac{3}{2}}^1]_{1_c}^1$	0 0 -1 1 1 -1	0 0 1 -1 -1 1
	$[[[QQ]_{\frac{3}{2}}^1 [\bar{Q}\bar{Q}]_{\frac{3}{2}}^0, \rho]_{\frac{3}{2}}^1]_{1_c}^1$	0 0 -1 1 1 -1	0 0 1 -1 -1 1
	$[[[QQ]_{\frac{3}{2}}^1 [\bar{Q}\bar{Q}]_{\frac{3}{2}}^0, \rho]_{\frac{3}{2}}^1]_{1_c}^1$	0 0 1 -1 1 -1	0 0 -1 1 -1 1
$1^{--}$	$[[[QQ]_{\frac{3}{2}}^0, \rho]_{\frac{3}{2}}^1 [\bar{Q}\bar{Q}]_{\frac{3}{2}}^1]_{1_c}^1$	$[[[QQ]_{\frac{3}{2}}^1 [\bar{Q}\bar{Q}]_{\frac{3}{2}}^1]_{1_c}^0, \lambda]_{1_c}^1$ (unit of $\frac{1}{\sqrt{6}}$ )	$[[[QQ]_{\frac{3}{2}}^1 [\bar{Q}\bar{Q}]_{\frac{3}{2}}^1]_{1_c}^0, \lambda]_{1_c}^1$
	$[[[QQ]_{\frac{3}{2}}^1 [\bar{Q}\bar{Q}]_{\frac{3}{2}}^0, \rho]_{\frac{3}{2}}^1]_{1_c}^1$	0 0 1 -1 1 -1	0 0 0 0 0 0
	$[[[QQ]_{\frac{3}{2}}^1 [\bar{Q}\bar{Q}]_{\frac{3}{2}}^0, \rho]_{\frac{3}{2}}^1]_{1_c}^1$	0 0 1 -1 -1 1	0 0 0 0 0 0
	$[[[QQ]_{\frac{3}{2}}^1 [\bar{Q}\bar{Q}]_{\frac{3}{2}}^0, \rho]_{\frac{3}{2}}^1]_{1_c}^1$	0 0 1 -1 -1 1	0 0 0 0 0 0
	$[[[QQ]_{\frac{3}{2}}^1 [\bar{Q}\bar{Q}]_{\frac{3}{2}}^0, \rho]_{\frac{3}{2}}^1]_{1_c}^1$	0 0 1 -1 1 -1	0 0 0 0 0 0
	$[[[QQ]_{\frac{3}{2}}^1 [\bar{Q}\bar{Q}]_{\frac{3}{2}}^0, \rho]_{\frac{3}{2}}^1]_{1_c}^1$	$[[[QQ]_{\frac{3}{2}}^0 [\bar{Q}\bar{Q}]_{\frac{3}{2}}^0]_{1_c}^0, \lambda]_{1_c}^1$ (unit of $\frac{1}{\sqrt{2}}$ )	$[[[QQ]_{\frac{3}{2}}^0 [\bar{Q}\bar{Q}]_{\frac{3}{2}}^0]_{1_c}^0, \lambda]_{1_c}^1$
	$[[[QQ]_{\frac{3}{2}}^1 [\bar{Q}\bar{Q}]_{\frac{3}{2}}^0, \rho]_{\frac{3}{2}}^1]_{1_c}^1$	0 0 -1 1 1 -1	0 0 0 0 0 0
	$[[[QQ]_{\frac{3}{2}}^1 [\bar{Q}\bar{Q}]_{\frac{3}{2}}^0, \rho]_{\frac{3}{2}}^1]_{1_c}^1$	0 0 -1 1 -1 1	0 0 0 0 0 0
	$[[[QQ]_{\frac{3}{2}}^1 [\bar{Q}\bar{Q}]_{\frac{3}{2}}^0, \rho]_{\frac{3}{2}}^1]_{1_c}^1$	0 0 -1 1 -1 1	0 0 0 0 0 0
	$[[[QQ]_{\frac{3}{2}}^1 [\bar{Q}\bar{Q}]_{\frac{3}{2}}^0, \rho]_{\frac{3}{2}}^1]_{1_c}^1$	0 0 -1 1 1 -1	0 0 0 0 0 0
	$[[[QQ]_{\frac{3}{2}}^1 [\bar{Q}\bar{Q}]_{\frac{3}{2}}^0, \rho]_{\frac{3}{2}}^1]_{1_c}^1$	$[[[QQ]_{\frac{3}{2}}^1 [\bar{Q}\bar{Q}]_{\frac{3}{2}}^1]_{1_c}^2, \lambda]_{1_c}^1$ (unit of $\frac{\sqrt{30}}{12}$ )	$[[[QQ]_{\frac{3}{2}}^1 [\bar{Q}\bar{Q}]_{\frac{3}{2}}^1]_{1_c}^2, \lambda]_{1_c}^1$ (unit of $\frac{3\sqrt{30}}{40}$ )
	$[[[QQ]_{\frac{3}{2}}^1 [\bar{Q}\bar{Q}]_{\frac{3}{2}}^0, \rho]_{\frac{3}{2}}^1]_{1_c}^1$	0 0 -1 1 -1 1	0 0 -1 1 -1 1
	$[[[QQ]_{\frac{3}{2}}^1 [\bar{Q}\bar{Q}]_{\frac{3}{2}}^0, \rho]_{\frac{3}{2}}^1]_{1_c}^1$	0 0 -1 1 1 -1	0 0 -1 1 1 -1
	$[[[QQ]_{\frac{3}{2}}^1 [\bar{Q}\bar{Q}]_{\frac{3}{2}}^0, \rho]_{\frac{3}{2}}^1]_{1_c}^1$	0 0 -1 1 1 -1	0 0 -1 1 1 -1
	$[[[QQ]_{\frac{3}{2}}^1 [\bar{Q}\bar{Q}]_{\frac{3}{2}}^0, \rho]_{\frac{3}{2}}^1]_{1_c}^1$	0 0 -1 1 -1 1	0 0 -1 1 -1 1
	$[[[QQ]_{\frac{3}{2}}^1 [\bar{Q}\bar{Q}]_{\frac{3}{2}}^0, \rho]_{\frac{3}{2}}^1]_{1_c}^1$		
$2^{-+}$	$[[[QQ]_{\frac{3}{2}}^0, \rho]_{\frac{3}{2}}^1 [\bar{Q}\bar{Q}]_{\frac{3}{2}}^1]_{1_c}^2$	$[[[QQ]_{\frac{3}{2}}^1 [\bar{Q}\bar{Q}]_{\frac{3}{2}}^1]_{1_c}^1, \lambda]_{1_c}^0$ (unit of $\frac{1}{2\sqrt{2}}$ )	$[[[QQ]_{\frac{3}{2}}^1 [\bar{Q}\bar{Q}]_{\frac{3}{2}}^1]_{1_c}^1, \lambda]_{1_c}^0$ (unit of $\frac{1}{20\sqrt{2}}$ )
	$[[[QQ]_{\frac{3}{2}}^1 [\bar{Q}\bar{Q}]_{\frac{3}{2}}^0, \rho]_{\frac{3}{2}}^1]_{1_c}^2$	0 0 -1 1 -1 1	0 0 1 -1 1 -1
	$[[[QQ]_{\frac{3}{2}}^1 [\bar{Q}\bar{Q}]_{\frac{3}{2}}^0, \rho]_{\frac{3}{2}}^1]_{1_c}^2$	0 0 1 -1 -1 1	0 0 -1 1 1 -1
	$[[[QQ]_{\frac{3}{2}}^1 [\bar{Q}\bar{Q}]_{\frac{3}{2}}^0, \rho]_{\frac{3}{2}}^1]_{1_c}^2$	0 0 1 -1 -1 1	0 0 -1 1 1 -1
	$[[[QQ]_{\frac{3}{2}}^1 [\bar{Q}\bar{Q}]_{\frac{3}{2}}^0, \rho]_{\frac{3}{2}}^1]_{1_c}^2$	0 0 -1 1 -1 1	0 0 1 -1 1 -1
$2^{--}$	$[[[QQ]_{\frac{3}{2}}^0, \rho]_{\frac{3}{2}}^1 [\bar{Q}\bar{Q}]_{\frac{3}{2}}^1]_{1_c}^2$	$[[[QQ]_{\frac{3}{2}}^1 [\bar{Q}\bar{Q}]_{\frac{3}{2}}^1]_{1_c}^2, \lambda]_{1_c}^2$ (unit of $\frac{\sqrt{6}}{4}$ )	$[[[QQ]_{\frac{3}{2}}^1 [\bar{Q}\bar{Q}]_{\frac{3}{2}}^1]_{1_c}^2, \lambda]_{1_c}^2$ (unit of $\frac{\sqrt{6}}{4}$ )
	$[[[QQ]_{\frac{3}{2}}^1 [\bar{Q}\bar{Q}]_{\frac{3}{2}}^0, \rho]_{\frac{3}{2}}^1]_{1_c}^2$	0 0 1 -1 1 -1	0 0 -1 1 -1 1
	$[[[QQ]_{\frac{3}{2}}^1 [\bar{Q}\bar{Q}]_{\frac{3}{2}}^0, \rho]_{\frac{3}{2}}^1]_{1_c}^2$	0 0 1 -1 -1 1	0 0 -1 1 1 -1
	$[[[QQ]_{\frac{3}{2}}^1 [\bar{Q}\bar{Q}]_{\frac{3}{2}}^0, \rho]_{\frac{3}{2}}^1]_{1_c}^2$	0 0 1 -1 -1 1	0 0 -1 1 1 -1
	$[[[QQ]_{\frac{3}{2}}^1 [\bar{Q}\bar{Q}]_{\frac{3}{2}}^0, \rho]_{\frac{3}{2}}^1]_{1_c}^2$	0 0 1 -1 1 -1	0 0 -1 1 -1 1



- arXiv:1909.13054 [hep-ph].
- [11] E. J. Eichten, K. Lane, and C. Quigg, *Phys. Rev. D* **69**, 094019 (2004), arXiv:hep-ph/0401210.
  - [12] Y. Iwasaki, *Prog. Theor. Phys.* **54**, 492 (1975).
  - [13] K.-T. Chao, *Z. Phys. C* **7**, 317 (1981).
  - [14] J. P. Ader, J. M. Richard, and P. Taxil, *Phys. Rev. D* **25**, 2370 (1982).
  - [15] S. Zouzou, B. Silvestre-Brac, C. Gignoux, and J. M. Richard, *Z. Phys. C* **30**, 457 (1986).
  - [16] L. Heller and J. A. Tjon, *Phys. Rev. D* **35**, 969 (1987).
  - [17] B. Silvestre-Brac, *Phys. Rev. D* **46**, 2179 (1992).
  - [18] V. Khachatryan *et al.* (CMS), *JHEP* **05**, 013 (2017), arXiv:1610.07095 [hep-ex].
  - [19] S. Durgut, “Search for Exotic Mesons at CMS (2018),” APS April Meeting 2018.
  - [20] R. Aaij *et al.* (LHCb), *JHEP* **10**, 086 (2018), arXiv:1806.09707 [hep-ex].
  - [21] Y. Bai, S. Lu, and J. Osborne, *Phys. Lett. B* **798**, 134930 (2019), arXiv:1612.00012 [hep-ph].
  - [22] M. N. Anwar, J. Ferretti, F.-K. Guo, E. Santopinto, and B.-S. Zou, *Eur. Phys. J. C* **78**, 647 (2018), arXiv:1710.02540 [hep-ph].
  - [23] W. Heupel, G. Eichmann, and C. S. Fischer, *Phys. Lett. B* **718**, 545 (2012), arXiv:1206.5129 [hep-ph].
  - [24] R. J. Lloyd and J. P. Vary, *Phys. Rev. D* **70**, 014009 (2004), arXiv:hep-ph/0311179.
  - [25] V. R. Debastiani and F. S. Navarra, *Chin. Phys. C* **43**, 013105 (2019), arXiv:1706.07553 [hep-ph].
  - [26] N. Barnea, J. Vijande, and A. Valcarce, *Phys. Rev. D* **73**, 054004 (2006), arXiv:hep-ph/0604010.
  - [27] A. V. Berezhnuy, A. K. Likhoded, A. V. Luchinsky, and A. A. Novoselov, *Phys. Rev. D* **84**, 094023 (2011), arXiv:1101.5881 [hep-ph].
  - [28] A. Esposito and A. D. Polosa, *Eur. Phys. J. C* **78**, 782 (2018), arXiv:1807.06040 [hep-ph].
  - [29] M. Karliner, J. L. Rosner, and T. Skwarnicki, *Ann. Rev. Nucl. Part. Sci.* **68**, 17 (2018), arXiv:1711.10626 [hep-ph].
  - [30] J. Wu, Y.-R. Liu, K. Chen, X. Liu, and S.-L. Zhu, *Phys. Rev. D* **97**, 094015 (2018), arXiv:1605.01134 [hep-ph].
  - [31] J.-M. Richard, A. Valcarce, and J. Vijande, *Phys. Rev. D* **95**, 054019 (2017), arXiv:1703.00783 [hep-ph].
  - [32] M.-S. Liu, Q.-F. Lü, X.-H. Zhong, and Q. Zhao, *Phys. Rev. D* **100**, 016006 (2019), arXiv:1901.02564 [hep-ph].
  - [33] A. Czarnecki, B. Leng, and M. B. Voloshin, *Phys. Lett. B* **778**, 233 (2018), arXiv:1708.04594 [hep-ph].
  - [34] C. Hughes, E. Eichten, and C. T. H. Davies, *Phys. Rev. D* **97**, 054505 (2018), arXiv:1710.03236 [hep-lat].
  - [35] W. Chen, H.-X. Chen, X. Liu, T. G. Steele, and S.-L. Zhu, *Phys. Lett. B* **773**, 247 (2017), arXiv:1605.01647 [hep-ph].
  - [36] A. V. Berezhnuy, A. V. Luchinsky, and A. A. Novoselov, *Phys. Rev. D* **86**, 034004 (2012), arXiv:1111.1867 [hep-ph].
  - [37] G.-J. Wang, L. Meng, and S.-L. Zhu, *Phys. Rev. D* **100**, 096013 (2019), arXiv:1907.05177 [hep-ph].
  - [38] R. Aaij *et al.* (LHCb), *Sci. Bull.* **65**, 1983 (2020), arXiv:2006.16957 [hep-ex].
  - [39] R. M. Albuquerque, S. Narison, A. Rabemananjara, D. Rabetiarivony, and G. Randriamanatrika, *Phys. Rev. D* **102**, 094001 (2020), arXiv:2008.01569 [hep-ph].
  - [40] M.-S. Liu, F.-X. Liu, X.-H. Zhong, and Q. Zhao, (2020), arXiv:2006.11952 [hep-ph].
  - [41] X. Jin, Y. Xue, H. Huang, and J. Ping, *Eur. Phys. J. C* **80**, 1083 (2020), arXiv:2006.13745 [hep-ph].
  - [42] Q.-F. Lü, D.-Y. Chen, and Y.-B. Dong, *Eur. Phys. J. C* **80**, 871 (2020), arXiv:2006.14445 [hep-ph].
  - [43] J. F. Giron and R. F. Lebed, *Phys. Rev. D* **102**, 074003 (2020), arXiv:2008.01631 [hep-ph].
  - [44] H. G. Dosch, S. J. Brodsky, G. F. de Téramond, M. Nielsen, and L. Zou, in *23rd High-Energy Physics International Conference in Quantum Chromodynamics: QCD20 - 35 years later* (2020) arXiv:2012.02496 [hep-ph].
  - [45] B.-C. Yang, L. Tang, and C.-F. Qiao, *Eur. Phys. J. C* **81**, 324 (2021), arXiv:2012.04463 [hep-ph].
  - [46] G. Huang, J. Zhao, and P. Zhuang, *Phys. Rev. D* **103**, 054014 (2021), arXiv:2012.14845 [hep-ph].
  - [47] C. Hughes, in *19th International Conference on B-Physics at Frontier Machines* (2021) arXiv:2101.08241 [hep-ph].
  - [48] R. N. Faustov, V. O. Galkin, and E. M. Savchenko, *Universe* **7**, 94 (2021), arXiv:2103.01763 [hep-ph].
  - [49] Z.-R. Liang, X.-Y. Wu, and D.-L. Yao, (2021), arXiv:2104.08589 [hep-ph].
  - [50] Q. Li, C.-H. Chang, G.-L. Wang, and T. Wang, (2021), arXiv:2104.12372 [hep-ph].
  - [51] Z.-H. Guo and J. A. Oller, *Phys. Rev. D* **103**, 034024 (2021), arXiv:2011.00978 [hep-ph].
  - [52] X.-K. Dong, V. Baru, F.-K. Guo, C. Hanhart, and A. Nefediev, *Phys. Rev. Lett.* **126**, 132001 (2021), arXiv:2009.07795 [hep-ph].
  - [53] B.-D. Wan and C.-F. Qiao, (2020), arXiv:2012.00454 [hep-ph].
  - [54] J.-W. Zhu, X.-D. Guo, R.-Y. Zhang, W.-G. Ma, and X.-Q. Li, (2020), arXiv:2011.07799 [hep-ph].
  - [55] F. Feng, Y. Huang, Y. Jia, W.-L. Sang, X. Xiong, and J.-Y. Zhang, (2020), arXiv:2009.08450 [hep-ph].
  - [56] X.-Y. Wang, Q.-Y. Lin, H. Xu, Y.-P. Xie, Y. Huang, and X. Chen, *Phys. Rev. D* **102**, 116014 (2020), arXiv:2007.09697 [hep-ph].
  - [57] R. Maciula, W. Schäfer, and A. Szczurek, *Phys. Lett. B* **812**, 136010 (2021), arXiv:2009.02100 [hep-ph].
  - [58] F. Feng, Y. Huang, Y. Jia, W.-L. Sang, and J.-Y. Zhang, (2020), arXiv:2011.03039 [hep-ph].
  - [59] V. P. Gonçalves and B. D. Moreira, *Phys. Lett. B* **816**, 136249 (2021), arXiv:2101.03798 [hep-ph].
  - [60] Y. Huang, F. Feng, Y. Jia, W.-L. Sang, D.-S. Yang, and J.-Y. Zhang, (2021), arXiv:2104.03887 [hep-ph].
  - [61] H. Mutuk, *Eur. Phys. J. C* **81**, 367 (2021), arXiv:2104.11823 [hep-ph].
  - [62] H.-X. Chen, W. Chen, X. Liu, and S.-L. Zhu, *Sci. Bull.* **65**, 1994 (2020), arXiv:2006.16027 [hep-ph].
  - [63] C. Becchi, J. Ferretti, A. Giachino, L. Maiani, and E. Santopinto, *Phys. Lett. B* **811**, 135952 (2020), arXiv:2006.14388 [hep-ph].
  - [64] H.-T. An, K. Chen, Z.-W. Liu, and X. Liu, *Phys. Rev. D* **103**, 074006 (2021), arXiv:2012.12459 [hep-ph].
  - [65] M. A. Bedolla, J. Ferretti, C. D. Roberts, and E. Santopinto, *Eur. Phys. J. C* **80**, 1004 (2020), arXiv:1911.00960 [hep-ph].
  - [66] Q.-F. Cao, H. Chen, H.-R. Qi, and H.-Q. Zheng, (2020), arXiv:2011.04347 [hep-ph].
  - [67] K.-T. Chao and S.-L. Zhu, *Sci. Bull.* **65**, 1952 (2020), arXiv:2008.07670 [hep-ph].
  - [68] R. N. Faustov, V. O. Galkin, and E. M. Savchenko, *Phys. Rev. D* **102**, 114030 (2020), arXiv:2009.13237 [hep-ph].
  - [69] C. Gong, M.-C. Du, B. Zhou, Q. Zhao, and X.-H. Zhong, (2020), arXiv:2011.11374 [hep-ph].

- [70] M. C. Gordillo, F. De Soto, and J. Segovia, *Phys. Rev. D* **102**, 114007 (2020), [arXiv:2009.11889 \[hep-ph\]](#).
- [71] M. Karliner and J. L. Rosner, *Phys. Rev. D* **102**, 114039 (2020), [arXiv:2009.04429 \[hep-ph\]](#).
- [72] H.-W. Ke, X. Han, X.-H. Liu, and Y.-L. Shi, (2021), [arXiv:2103.13140 \[hep-ph\]](#).
- [73] W. Lucha, D. Melikhov, and H. Sazdjian, (2021), [arXiv:2102.02542 \[hep-ph\]](#).
- [74] Y.-Q. Ma and H.-F. Zhang, (2020), [arXiv:2009.08376 \[hep-ph\]](#).
- [75] J.-M. Richard, *Sci. Bull.* **65**, 1954 (2020), [arXiv:2008.01962 \[hep-ph\]](#).
- [76] J. Sonnenschein and D. Weissman, *Eur. Phys. J. C* **81**, 25 (2021), [arXiv:2008.01095 \[hep-ph\]](#).
- [77] Z.-G. Wang, *Int. J. Mod. Phys. A* **36**, 2150014 (2021), [arXiv:2009.05371 \[hep-ph\]](#).
- [78] J.-Z. Wang, D.-Y. Chen, X. Liu, and T. Matsuki, *Phys. Rev. D* **103**, 071503 (2021), [arXiv:2008.07430 \[hep-ph\]](#).
- [79] Z.-G. Wang, (2021), [arXiv:2104.12090 \[hep-ph\]](#).
- [80] X.-Z. Weng, X.-L. Chen, W.-Z. Deng, and S.-L. Zhu, *Phys. Rev. D* **103**, 034001 (2021), [arXiv:2010.05163 \[hep-ph\]](#).
- [81] G. Yang, J. Ping, and J. Segovia, (2021), [arXiv:2104.08814 \[hep-ph\]](#).
- [82] Z.-H. Yang, Q.-N. Wang, W. Chen, and H.-X. Chen, (2021), [arXiv:2102.10605 \[hep-ph\]](#).
- [83] J.-R. Zhang, *Phys. Rev. D* **103**, 014018 (2021), [arXiv:2010.07719 \[hep-ph\]](#).
- [84] Z. Zhao, K. Xu, A. Kaewsnod, X. Liu, A. Limphirat, and Y. Yan, (2020), [arXiv:2012.15554 \[hep-ph\]](#).
- [85] J. Zhao, S. Shi, and P. Zhuang, *Phys. Rev. D* **102**, 114001 (2020), [arXiv:2009.10319 \[hep-ph\]](#).
- [86] R. Zhu, *Nucl. Phys. B* **966**, 115393 (2021), [arXiv:2010.09082 \[hep-ph\]](#).
- [87] T. Barnes, S. Godfrey, and E. S. Swanson, *Phys. Rev. D* **72**, 054026 (2005), [arXiv:hep-ph/0505002](#).
- [88] S. Godfrey and N. Isgur, *Phys. Rev. D* **32**, 189 (1985).
- [89] P. Zyla *et al.* (Particle Data Group), *PTEP* **2020**, 083C01 (2020).
- [90] E. Hiyama, Y. Kino, and M. Kamimura, *Prog. Part. Nucl. Phys.* **51**, 223 (2003).
- [91] E. Hiyama and M. Kamimura, *Front. Phys. (Beijing)* **13**, 132106 (2018), [arXiv:1809.02619 \[nucl-th\]](#).
- [92] B. Silvestre-Brac, *Few Body Syst.* **20**, 1 (1996).
- [93] T. Yoshida, E. Hiyama, A. Hosaka, M. Oka, and K. Sadato, *Phys. Rev. D* **92**, 114029 (2015), [arXiv:1510.01067 \[hep-ph\]](#).